# The $\beta$-spectrum of $^{35}$S and search for the admixture of heavy neutrinos

E. Holzschuh, L. Palermo, H. Stüssi, P. Wenk

*Physik-Institut der Universität Zürich, CH-8057 Zürich, Switzerland*



**Abstract**

The $\beta$-spectrum of $^{35}$S has been measured with high statistical precision. A total of $2.2 \times 10^{10}$ events have been accumulated with a signal to background ratio of $10^3$ or better. A systematic search for neutrino mixing has been performed for assumed neutrino masses up to 105 keV. In the mass range 10 to 90 keV, an upper limit around $10^{-3}$ or less was set for the mixing probability.

*Key words:* Neutrino masses; $\beta$-spectroscopy.
*PACS:* 14.60.Pq; 23.40.-s

## 1 Introduction

In a previous publication [1] we presented measurements of the $^{63}$Ni $\beta$-spectrum and a search for neutrino mixing with assumed masses up to 33 keV. In this letter we extend the search to masses up to 105 keV using the $\beta$-decay of $^{35}$S.

Our method is simple in principle. We use a large magnetic spectrometer with high resolution. If neutrino mixing would exist for sufficiently large neutrino masses, a kink-like structure in a $\beta$-spectrum is predicted [2]. This would be a unique signature in an otherwise smooth spectrum if measured with high resolution. At the same time other deviations from the theoretically expected spectrum shape may also be detected.

## 2 Experimental

A detailed description of the experiment and the results of test measurements have been given previously [3]. The method to produce the $^{35}$S source has

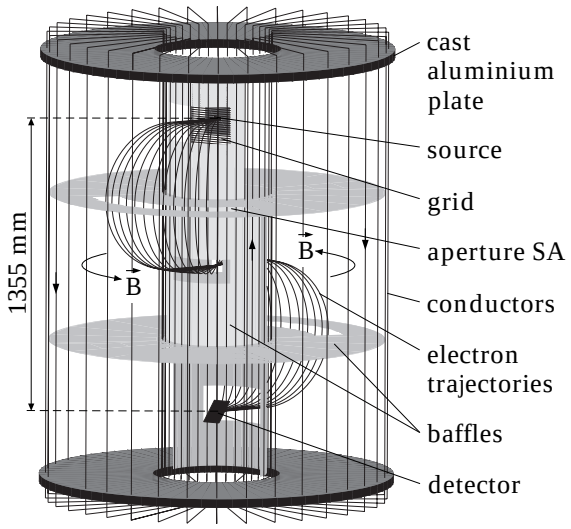


Fig. 1. Simplified view of the spectrometer.

been described in Ref.s [4,5]. The measurements reported in this letter were performed in a similar way as before [1]. Therefore only a brief overview is given in this section.

### *2.1 Spectrometer*

The instrument used is an iron-free magnetic $\beta$-spectrometer of the Tret'yakov type with electrostatic acceleration at the source. A simplified overview is given in Fig. 1. A toroidal magnetic field is produced by a set of 72 rectangular current loops. The source and the detector are placed on the symmetry axis of the spectrometer. Electrons from the source are transported through a set of baffles in two 180° bends to the detector.

The source was mounted on a plate which was surrounded by a box-like grid. The grid was made of aluminium wire with 1 mm pitch. Initially the wire diameter was 17.5 $\mu$m. During the measurements (run C) the wire broke and was replaced by a slightly thicker one (20.0 $\mu$m diameter). An electrostatic acceleration field between source and grid was produced by applying a negative high voltage $V_S$ to the source holder while keeping the grid at a potential near ground.

The focal plane of the spectrometer is inclined by an angle of 48.5° with respect to the symmetry axis. A large silicon strip detector, consisting of four silicon plates with a sensitive area of $8.0 \times 3.05\,\mathrm{cm}^2$ each, was mounted in the focal plane. The strip pitch and thus the position resolution was 1.27 mm.

Each detector strip was read out by a separate electronic channel, consisting of a charge sensitive preamplifier, a shaping amplifier and an 11 bit ADC.

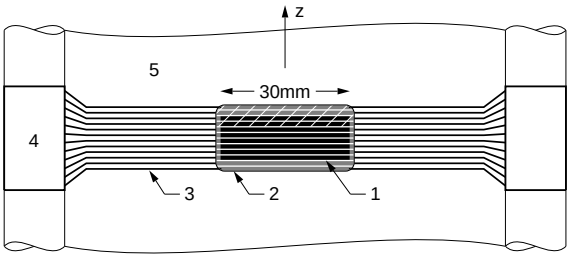


Fig. 2. Layout of the $^{35}$S source. (1) Active area, (2) thin foil stretched over an opening, (3) electrical connections, (4) insulator and support frame, (5) copper-plated board. The vertical direction through the centre coincides with the spectrometer axis. The hatched area has been covered during run C to fix a hole in the foil.

Electrons hitting the detector near the borderline of two adjacent strips were identified with coincidence logic. The total dead time was measured to be $9.4 \pm 0.3\,\mu$s, being within uncertainties the same for all channels. Some of the detector strips or preamplifiers had excessive noise and were shut off. The average pulse height resolution of the remaining channels was 5.5 keV (FWHM).

### *2.2 Source*

A segmented source was used with a layout shown in Fig. 2. The $^{35}$S activity was spread on eight electrically conducting strips ($30 \times 1$ mm) with 1.3 mm pitch. The active and four non-active strips were connected to a resistor chain. During measurements a voltage was applied to the chain, producing a potential gradient which compensated the vertical source extent.

The source was built up in the following way. First, a thin foil [6] of polyimide (Kapton) was glued onto a frame of glass-fibre epoxy. The foil thickness as determined by $\alpha$-spectroscopy was $28 \pm 3\,\mu$g/cm$^2$ or 1970 Å assuming a density of 1.42 g/cm$^3$. Next, the pattern of 12 conducting strips was produced by vacuum-evaporation of aluminium through a mask. The thickness of the aluminium layer was 300 Å. Then a 50 Å thick layer of copper was deposited on 8 of these strips through another mask.

The $^{35}$S activity was brought on the support foil by a chemical reaction of $H_2{}^{35}S$ gas with the copper layer [4]. The active material was purchased in the form of $Na_2{}^{35}S$ dissolved in 0.1 M NaOH and had a specific activity of 50 Ci/mmol. The active solution and the foil were put into a reaction vessel filled with argon. $H_2{}^{35}S$ gas was released by decomposing the sodium sulfide with sulfuric acid. The reaction products were copper sulfides and some copper (oxide) sulfate.

The activity of the completed source was measured with an ion chamber to

be $5.3 \pm 0.2\,\mathrm{mCi}$. Using the amount of deposited copper, the thickness of the active layer was estimated to be $(5 \pm 1)\mu\mathrm{g/cm}^2$.

The rupture of the grid wire mentioned before led to a hole in the source foil. This was fixed by glueing a plate onto the foil and board. The affected part of the source is indicated by the hatched area in Fig. 2.

## 3 Measurements

The measurement procedure of a $\beta$-spectrum was basically the same as used previously [1]. The current through the spectrometer coil was set to a constant analysing energy $E_{\mathrm{mag}}$. The spectrum was scanned by varying the high voltage $V_{\mathrm{S}}$ applied to the source in equal steps. In order to avoid that drifts in the apparatus or the decay of the source would affect the measured spectrum shape, the scanning was done as interlaced up-down sweeps. The time interval between changing from an up to a down sweep and vice versa was approximately one minute. Several hours were needed for a complete up-down sweep.

For each detected electron the measured pulse height, the number of the detector strip being hit, and two coincidence bits were recorded on magnetic tape. Histograms were built off-line. The pulse height was only used for applying cuts. Events with coincidence bits set were rejected, thus avoiding double counting. From the strip number a coordinate $z$ along the spectrometer axis and with zero point at the detector centre was determined. Then an energy

$$E = E_{\mathrm{mag}} - e|V_{\mathrm{S}}| + zD_E \tag{1}$$

was assigned to each event, where $D_E$ denotes the energy dispersion. The events were summed into bins assuming nominal values for $E$ to ensure the same width for all bins of a spectrum. The energy assigned to a bin was taken to be the average of all events in a bin using the measured values of $E_{\mathrm{mag}}$ and $V_{\mathrm{S}}$. The standard deviation of the single event energies for one bin varied between 2 and 4 eV depending on settings. This was small enough to be negligible.

The total energy range measured extended from 56.0 to 172.8 keV. This range was divided in five overlapping intervals for several reasons. The high voltage which could be applied to the source without stability problems was limited to approximately 40 kV. The correction for the solid angle accepted by the spectrometer at the source (see Ref. [3] and section 4.2), becomes large and therefore difficult to compute at high acceleration voltages. A summary of the settings is given in Tab. 1.

Table 1
Settings for the measurements of the $^{35}$S $\beta$-spectrum.

| Run | | A | B | C | D | E |
|---|---|---|---|---|---|---|
| $E_{\mathrm{mag}}$ (keV) | | 179.9 | 155.5 | 129.9 | 109.5 | 82.2 |
| Energy range (keV) | $E_{\mathrm{min}}$ | 145.2 | 120.0 | 93.6 | 72.7 | 56.0 |
| | $E_{\mathrm{max}}$ | 172.8 | 149.2 | 124.5 | 104.9 | 78.6 |
| Resolution, FWHM (eV) | | 210 | 185 | 157 | 134 | 103 |
| Dispersion (eV/mm) | | 143 | 126 | 107 | 91 | 70 |
| Bin width (eV) | | 121 | 106 | 90 | 77 | 59 |

Table 2
Pulse height cuts (keV) used in the analysis.

| Run | A | B | C | D | E |
|---|---|---|---|---|---|
| Cut 1 | 44 | 33 | 28 | 26 | 26 |
| Cut 2 | 77 | 66 | 55 | 46 | 34 |
| Cut 3 | 110 | 99 | 83 | 68 | 51 |
| Cut 4 | 143 | 132 | 106 | 84 | 60 |
| Max | 204 | 176 | 149 | 126 | 101 |

The measurements were started with run A and then runs B, C, D and E were performed in sequence. The total time required for the measurements was about 200 days or 2.3 half-lives of $^{35}$S. The strong increase of the $\beta$-spectrum with decreasing energy could thus be compensated somewhat. For the same reason the range of each run was divided in two (three for B) subintervals with 12 s counting time per step at high and 6 s at low energies (16, 8, 4 s for B). The different counting times were taken into account by scaling the histograms such that the scale factor was 1 at the high energy subintervals.

Histograms were built with four different pulse height cuts for each run. The cuts are listed in Tab. 2. A common upper limit for all cuts of a run was chosen such that only background events would be detected above this limit.

A summary of the counts and rates of the measurements is given in Tab. 3. The total number of events for all runs is $2.2 \times 10^{10}$ for cut 1. The number of events for the narrowest cut 4 is about 30 % less. This is due to the electrons which were backscattered from the detector, thereby depositing only part of their energy. The data of run A and cut 4 are shown in Fig. 3.

The background was mainly caused by cosmic ray muons and by a small contamination with $^{35}$S, which occurred initially after inserting the source

Table 3
Summary of counts and rates of the measurements.

| Run | | A | B | C | D | E |
|---|---|---|---|---|---|---|
| No. up-down sweeps | | 616 | 417 | 188 | 77 | 43 |
| Total counts ($10^9$) | | 2.12 | 7.70 | 6.02 | 3.88 | 2.53 |
| Max. rate / strip ($s^{-1}$) | | 80 | 191 | 170 | 203 | 256 |
| Background / strip ($s^{-1}$) | Cut 2 | 0.058 | 0.074 | 0.077 | 0.086 | 0.102 |
| | Cut 4 | 0.006 | 0.007 | 0.015 | 0.026 | 0.045 |

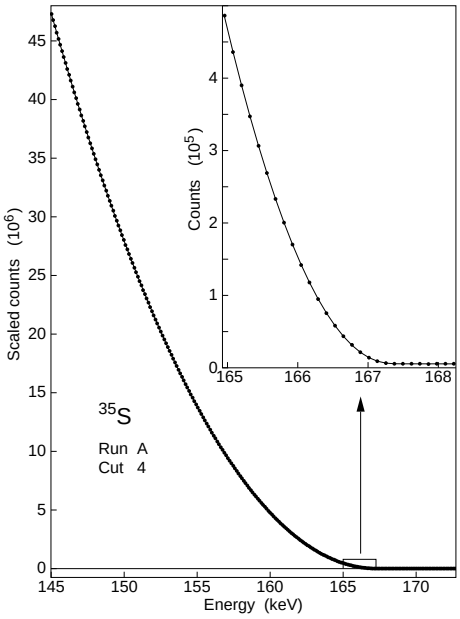


Fig. 3. $\beta$-spectrum from run A and a best fit. The inset shows the endpoint region on an expanded scale. All error bars are much smaller than the size of the data points.

into the spectrometer [4]. For run A, the background could be determined from the histogram as the measured range extends well above the spectrum endpoint ($E_0 \simeq 167.3\,\mathrm{keV}$). For the other runs, the regular measurements were interrupted each day and the background counted for typically 20 min by setting the spectrometer to an energy of 180 keV. The background rates were determined by applying the cuts and averaging the counts over the time of a run. The results for two cuts and the maximal rates of signal counts are given in Tab. 3. The background rates were strongly cut-dependent but the

ratio of maximal signal rate to background was always larger than $10^3$.

## 4 Simulation

A fairly complete simulation of the experiment was performed employing the same method as described in Ref. [3] and used previously [1]. The energy distribution of the simulated source was assumed to be a constant and the results were scaled as required.

### *4.1 Scattering*

Electrons, which were scattered in the spectrometer and detected, caused a distortion in the measured $\beta$-spectrum. In order to have a correction for this effect, a Monte Carlo simulation was performed for each experimental run. Energy spectra were generated for scattered and for not-scattered electrons hitting the detector by scaling each event with the theoretical $\beta$-spectrum of $^{35}$S.

The objects in the spectrometer which contributed most to the number of scattered and detected electrons were the source holder, the acceleration grid, and the detector and its support. Scattering from the current conductors was relatively small and from the baffle edges it was negligible.

The surface of the source foil, for practical reasons of the source production, was approximately 0.5 mm below the surface of the source board (see Fig. 2). The resulting edges contributed significantly to scattering. Backscattering from the source foil was a comparatively minor effect. Scattering from the plate, inserted during run C (see section 2.2), was also significant and included in the simulation for the affected runs. In all, the largest effect was due to scattering at the grid.

The fraction of electrons being scattered somewhere in the source region and detected was unaffected by the cuts. This is because such electrons must have had nominal energies after scattering to pass through the spectrometer and to reach the detector. In contrast, electrons scattered in the detector region were strongly suppressed by applying the narrowest cut.

The number of simulated events hitting the detector was of order $10^7$ for each of the five runs. Using cut 4, the fraction of scattered electrons was $6.4 \times 10^{-3}$ for run A, increasing monotonically for the runs with lower energies up to a value of $2.5 \times 10^{-2}$ for run E. These fractions were larger for wider cuts, the relative increase being roughly 40 % for cut 1.

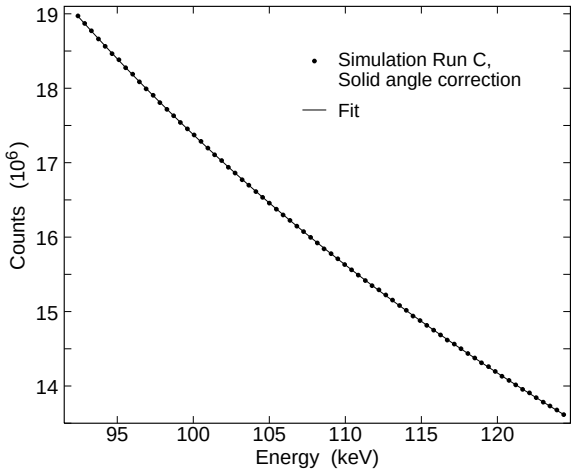


Fig. 4. Simulated solid angle correction (points) for run C and a best fit (line).

### *4.2 Solid angle correction*

The solid angle, accepted by the spectrometer at the source, increases with increasing acceleration voltage $V_S$. This effect was naturally included in the simulation. In addition a simulation with very high statistical precision was performed for run C. Scattering was turned off to speed up the computation. The resulting histogram is shown in Fig. 4 and contains $1.2 \times 10^9$ events, i.e. the same order of magnitude as the experimental $\beta$-spectra. The computing time was equivalent to 150 days of a 300 MHz Pentium-II processor.

The simulated data were fitted to the formula [3]

$$S(E) = \frac{Z}{\varphi} \arcsin(Z \sin \varphi), \tag{2}$$

where $Z := p_{\mathrm{mag}}/p$ is the ratio of the spectrometer momentum setting to the electron momentum at the source. A very good fit was obtained with $\chi^2 = 352$ for 361 degrees of freedom. The effective opening angle was fitted to be $\varphi = 16.98 \pm 0.13°$. This is roughly a factor of two more precise than what would be obtained by fitting the correction to an experimental $\beta$-spectrum.

## 5 Analysis and results

### *5.1 Spectrum shape*

The model for fitting the data was constructed similar as before [1]. A two-state neutrino mixing scheme with neutrino masses $m_1$ and $m_2$ was assumed.

For this case, the theoretical $\beta$-spectrum is expected to have the form [2]

$$f_m(E) = (1 - |U_{e2}|^2) f(E_0, m_1, E) + |U_{e2}|^2 f(E_0, m_2, E)\,. \qquad (3)$$

One neutrino mass was assumed to be negligibly small as indicated by recent tritium experiments [7]. Consequently $m_1$ was set to zero in the analysis. The function $f(E_0, m, E)$ describes a $\beta$-spectrum for a given neutrino mass $m$ and an extrapolated endpoint $E_0$. It was computed in the following way.

To a first approximation, the Fermi function for a point charge nucleus with infinite mass was used [8]. Corrections for finite nuclear size and recoil were applied using the parameterization from Ref. [9]. The relative variation of the combined correction was $3.5 \times 10^{-4}$ over the measured energy range.

Radiative corrections were included up to order $\alpha$ [10]. Over the energy range where the measured data are significantly above background, this correction varied by $9 \times 10^{-3}$.

Electrostatic screening due to the atomic electrons was taken into account using the Rose prescription [11] with a screening potential of 1643 eV. The correction agreed with tabulated values [12] within the precision of the table ($10^{-4}$) and increased by $3.6 \times 10^{-3}$ from 56 keV to the endpoint.

The exchange correction, due to the fact that $\beta$-particles and atomic electrons are indistinguishable, were taken from Ref. [13]. This correction decreased by $1.7 \times 10^{-3}$ from 56 keV to the endpoint.

The excitation probabilities for the atomic electrons in the final state were taken from Ref. [14]. The mean of the atomic excitation energies was computed using a Dirac-Fock program [15] to be 65 eV and the excitation energies were adjusted correspondingly. This was not a unambiguous procedure and large errors had to be assumed.

The following corrections to the fitted model are experimental. The spectrometer resolution function for each run was determined by simulation and taken into account by convolution with the theoretical spectrum shape. The widths are given in Tab. 1.

The energy loss due to inelastic scattering in the source layer was a small but complicated correction. The differential cross sections for K and L excitations in Cu and S were computed using the programs from Ref. [16]. For the cross sections of the more weakly bound electrons, the model of Ref. [17] was used. The mean energy loss varied from 11 eV to 5.6 eV over the measured energy range, agreeing within few percents with computations using table values [18]. The fraction of $\beta$-particles interacting inelastically, 6.6 to 3.1 %, was small

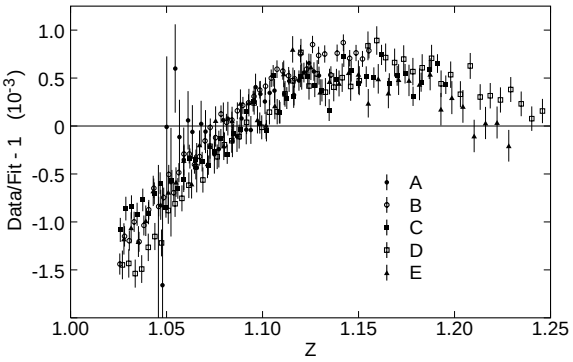


Fig. 5. Ratio of the data and a minimal fit (see text). Between five and nine original data points were added for this plot resulting in approximately the same bin width (600 eV) for all runs.

enough to justify the neglect of multiple scattering in the source layer and the correction could be taken into account by one convolution.

The computed scattering distributions (section 4.1) were parametrized using an expression of the form

$$(1 + c_1\epsilon^2 + c_2\epsilon^3 + \cdots)\,\Theta(\epsilon)\epsilon^2 \otimes g(\epsilon) \tag{4}$$

with $\epsilon := E_0 - E$. Here $\otimes$ denotes the analytic convolution of a rough approximation of the $\beta$-spectrum ($\Theta(\epsilon)\epsilon^2$) with a broad distribution being either a gaussian or an exponential $\exp(-\alpha|\epsilon|)$. The standard deviation of $g(\epsilon)$ was found to be 4 keV (run A). In this way a good approximation was obtained both for the effect of scattering in the detector region which caused electrons to be detected at energies way above the endpoint and also in the spectrum region at low energies. The result was scaled with the total number of signal events and added to the fitted function as a fixed correction. The type of parameterization did not affect the fit of the $\beta$-spectra in any significant way.

Lost events due to electronic dead time were taken into account by the appropriate correction factor. Using the rates in Tab. 3 this correction was at most $2.4 \times 10^{-3}$. Background was assumed to be independent of energy [1]. For run A, the background was fitted to the data. For all other runs, the measured background rates (section 3) were scaled with the measuring times and added as fixed corrections.

The solid angle correction was first assumed to be the factor given by Eq. 2 as it was indeed a very good approximation in our previous measurement [1]. Fits obtained in this way turned out to produce inconsistent results for the present case, however. That is to say, the slopes of the spectra at energies where the ranges of two runs overlap, were not exactly equal, the difference increasing systematically with lower energies. Comparing the data as a function of the variable $Z$ instead of $E$, most of the differences disappeared. This is

Table 4
Fitted values of $\chi^2$ for cuts 2 and 4 and the numbers of degrees of freedom Nof.

| Run | $\chi^2$ (Cut 2) | $\chi^2$ (Cut 4) | Nof |
|---|---|---|---|
| A | 313 | 235 | 230 |
| B | 254 | 268 | 277 |
| C | 381 | 406 | 344 |
| D | 462 | 457 | 419 |
| E | 362 | 375 | 384 |
| All | 1772 | 1740 | 1635 |

demonstrated in Fig. 5. Plotted is the ratio of all data and a fit on a common $Z$ axis. All corrections discussed so far were included in the fit with the solid angle correction taken from the simulations. The free parameters of the fit were a minimal set, consisting of the endpoint energy $E_0$ and one spectrum amplitude for each run. The size of the deviations from the nominal value 1 is of order $10^{-3}$, but their shapes are seen to be approximately the same for all five spectra.

This suggests that the assumption of a flat surface, formed by source board and foil, as it was indeed the case previously [1], was not good enough for the present measurements. The edges of the source, due to the 0.5 mm height difference of foil and board (section 4.1), caused a small-scale distortion of the electric field which however was not practical to be included in the simulations. It can be shown that the solid angle correction in this case is approximately still a function of $Z$ only. Therefore Eq. 2 was used as computed (i.e. $\varphi = 17°$) and corrected by a factor of the form

$$1 + \alpha_1(Z-1) + \alpha_2(Z-1)^2 + \alpha_3(Z-1)^3 \qquad (5)$$

with free parameters $\alpha_i$. For runs A and B, due to the relatively small range of $Z$, a linear correction would have been sufficient, but for consistency all five runs were treated the same way.

### *5.2 Results*

The data were analysed by global fits to the combined set of all spectra. First, no neutrino mixing was assumed and fits were made separately for all four cuts to test internal consistency. Values for the global $\chi^2$ and the contributions of the individual runs are given in Tab. 4 for cuts 2 and 4. The differences between data and fit, scaled with the standard deviations, are

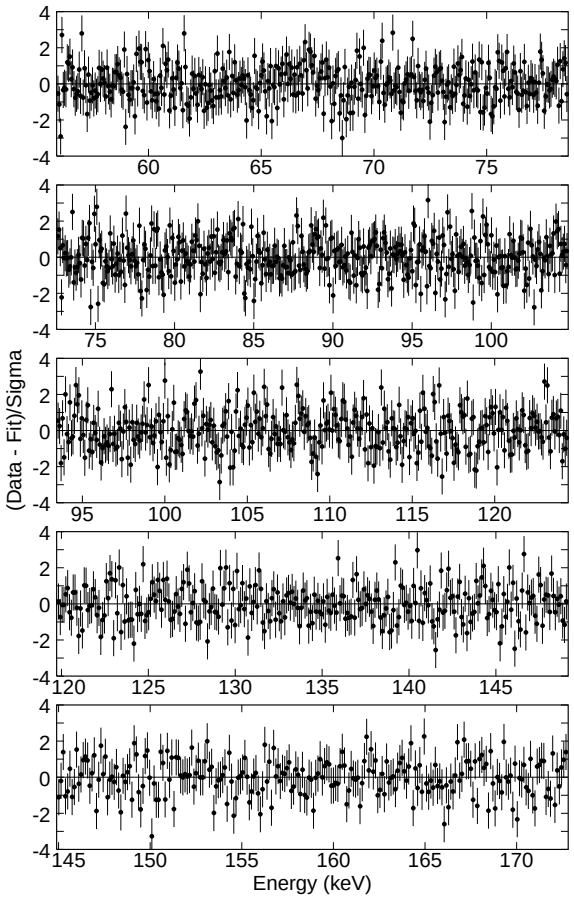


Fig. 6. Data minus the best fit divided by the statistical standard deviation for the five $^{35}$S runs (cut 4 and no mixing).

plotted in Fig. 6 for cut 4. There are no indications for systematic effects. The same applies for the other cuts except run A, were systematic deviations exist around the endpoint for cuts 1 and 2 (cut 2 being the worst). Also the fitted value of $E_0$ moved systematically by some 3 eV with the cut number. These observations are interpreted to indicate that the accuracy of the simulation of the complicated scattering in the detector region is somewhat marginal. However, such scattered electrons are strongly suppressed by the narrowest cut. For this reason and also because of the greatly reduced background, the further analysis was performed with cut 4.

The value of the endpoint parameter $E_0$ was determined by the data (predominantly run A) with a statistical uncertainty of 0.4 eV. The systematic uncertainties were much larger, being dominated by the spectrometer calibration [1] whereas uncertainties due to energy loss in the source and the final states where comparatively small. Our result is

$$E_0 = 167334 \pm 27\,\mathrm{eV}. \tag{6}$$

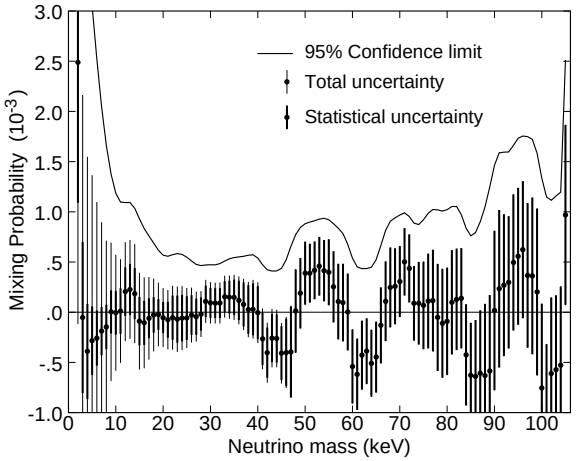


Fig. 7. Best fit (points) of the mixing probability as a function of assumed neutrino mass. The error bars combine statistical and systematic errors. The thick part of the error bars represents the statistical errors only. The solid line is an upper limit at 95 % confidence.

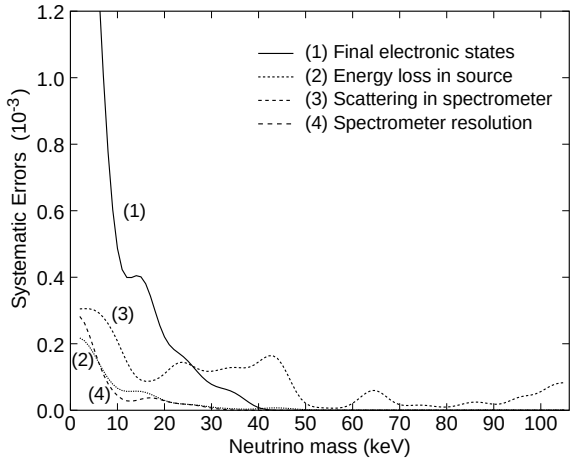


Fig. 8. Estimate of systematic errors ($1\sigma$) of the mixing probability as a function of the assumed neutrino mass.

In the past, many measurements of $E_0$ have been reported, partly with large discrepancies (see Ref. [5] for references). The results with the smallest claimed errors range from $167067 \pm 65\,\mathrm{eV}$ [19] to $167560 \pm 30\,\mathrm{eV}$ [20]. Hence a comparison is not easy. Our value is in marginal agreement with an average, $E_0 = 167180 \pm 120\,\mathrm{eV}$, recommended in [21].

Neutrino mixing was searched for using Eq. 3 with the mixing probability $|U_{e2}|^2$ as an additional free parameter. The assumed neutrino mass $m_2$ was varied in steps in the range 2 to 105 keV. The results are shown in Fig. 7. There is no indication for neutrino mixing in this range. We note that the values of $|U_{e2}|^2$ in Fig. 7 are not statistically independent as they were derived from the same data.

Systematic uncertainties for $|U_{e2}|^2$ were determined by varying the various corrections in the fitted model within the estimated errors and fitting the data again. The differences to the standard model were taken as $1\,\sigma$ errors for $|U_{e2}|^2$. The largest of these are plotted in Fig. 8.

For small values of $m_2$, the theoretical uncertainties due to the excitation of final electronic states is dominant. The plotted curve (1) combines these errors. It was obtained by changing the probabilities for K and L excitations by some 50 % in such a way that the mean excitation energy remained constant and by changing the excitation energies such that their mean varied by 5 eV while keeping the probabilities constant.

The effects of energy loss on the spectrum shape was similar but small because of the thin source. Curve (2) in Fig. 8 was obtained by assuming the source to be 30 % thicker than estimated.

The uncertainty due to scattering was determined by changing the amplitude of the simulated corrections by 25 %. A check was made by comparing the results for cut 3 and 4. The differences were compatible with statistical fluctuations due to the approximately 8 % larger number of events for cut 3, excepting the results for $m_2 < 10\,\mathrm{keV}$. But also for these small values of $m_2$, the effect of the 25 % amplitude change was larger.

The widths of the resolution functions for all five runs were changed by 5 %, but a significant uncertainty was only caused for small values of $m_2$. Uncertainties due to errors of the measured backgrounds (5 %) and of the dead time (0.3 $\mu$s) were $10^{-5}$ or less and are therefore not shown.

The total uncertainties for $|U_{e2}|^2$, shown in Fig. 7 as thin error bars, were obtained by adding the statistical and all systematic uncertainties quadratically. Upper limits for the mixing probabilities at 95 % confidence were computed using the method of the particle data group [22]. This is our final result, shown in Fig. 7 as solid line.

Searches for neutrino mixing in $\beta$-decay have been performed previously mainly in connection with the 17 keV neutrino (see Ref. [23] for a review). For neutrino masses up to about 50 keV, limits for $|U_{e2}|^2$ down to $10^{-3}$ have been claimed. In the range 50 to 100 keV, a measurement of $^{64}$Cu gave limits from 2 % to 1 % [24]. For larger neutrino masses, up to 6.8 MeV, limits at the level around $2 \times 10^{-3}$ have been deduced from the $\beta$-decay of $^{20}$F and the ft-values of the superallowed Fermi decays [25].

## 6 Conclusion

The $\beta$-spectrum of $^{35}$S has been measured with high precision and a systematic search for neutrino mixing with masses up to 105 keV has been performed. For assumed neutrino masses in the range 10 to 90 keV upper limits around $10^{-3}$ or less were set, extending our previous result with $^{63}$Ni to larger mass values.

The measured shape of the $^{35}$S $\beta$-spectrum was found to agree well with the theoretical predictions. In the endpoint region, however, sizeable uncertainties do still exist due to the excitation of electronic final states.


## Acknowledgements

This work has been supported by the Swiss Science Foundation and by the Paul Scherrer Institute (PSI) which is gratefully acknowledged. We thank R. Alberto for the help making the source.


## References


[1] E. Holzschuh, W. Kündig, L. Palermo, H. Stüssi, P. Wenk, Phys. Lett. B 451 (1999) 247.

[2] R.E. Shrock, Phys. Lett. B 96 (1980) 159.

[3] E. Holzschuh, W. Kündig, L. Palermo, H. Stüssi, P. Wenk, Nucl. Instr. Meth. A 423 (1999) 52.

[4] L. Palermo, E. Holzschuh, W. Kündig, P. Wenk, R. Alberto, Nucl. Instr. Meth. A 423 (1999) 337.

[5] L. Palermo, Dissertation, University of Zürich, 1998.

[6] P. Wenk, Dissertation, University of Zürich, 1998.

[7] C. Caso et al. (Particle Data Group), Euro. Phys. J. C 3 (1998) 1.

[8] H. Behrens, W. Bühring, Electron Radial Wave Functions and Nuclear Beta-decay, Clarendon Press, Oxford, 1982.

[9] D.H. Wilkinson, Nucl. Instr. Meth. A 290 (1990) 509.

[10] A. Sirlin, Phys. Rev. 164 (1967) 1767.

[11] M. Rose, Phys. Rev. 49 (1936) 727.

[12] H. Behrens, J. Jaenecke, in Landolt-Börnstein, New Series, Vol. 4, Numerical tables for beta-decay and electron capture, Springer Verlag, Berlin, 1969.

[13] M.R. Harston, N.C. Pyper, Phys. Rev. A 45 (1992) 6282.

[14] T.A. Carlson et al., Phys. Rev. 169 (1968) 27.

[15] A.L. Ankudinov et al., Comput. Phys. Commun. 98 (1996) 359.

[16] R.F. Egerton, Electron energy loss spectroscopy in the electron microscope, 2nd Ed., Plenum Press, New York, 1996.

[17] D. Liljequist, J. Phys. D 16 (1983) 1567.

[18] M.J. Berger, S.M. Selzer, ICRU report 37, 1984.

[19] A. Hime and N.A. Jelley, Phys. Lett. B 257 (1991) 441.

[20] M. Chen et al., Phys. Rev. Lett. 69 (1992) 3151.

[21] R.B. Firestone, Table of Isotopes (John Wiley & Sons, New York 1996).

[22] H. Hikara et al. (Particle Data Group), Phys. Rev. D 45 (1992) III.32.

[23] F.E. Wietfeldt and E.B. Norman, Phys. Rep. 273 (1996) 149.

[24] K. Schreckenbach et al., Phys. Lett. B 129 (1983) 265.

[25] J. Deutsch, M. Lebrun, and R. Prieels, Nucl. Phys. A 518 (1990) 149.